SPIN LOSS ANALYSIS OF FRICTION DRIVES: SPHERICAL AND SEMI-SPHERICAL CVT

J. KIM[1]* and K. H. CHOI[2]

[1]*School of Mechanical and Aerospace Engineering, Seoul National University, Seoul 151-742, Korea
[2]Korea Railroad Research Institute, Woulam-dong, Uiwang-si, Gyeonggi-do 413-050, Korea

ABSTRACT–This article deals with the spin loss analysis of friction drive CVTs, especially for the cases of S-CVT and SS-CVT. There are two main sources of power loss resulting from slippage in the friction drive CVT, spin and slip loss. Spin loss, which is also a main design issue in traction drives, results from the elastic contact deformation of rotating bodies having different rotational velocities. The structure and operating principles of the S-CVT and SS-CVT are first reviewed briefly. And to analyze the losses resulting from slippage, we reviewed previous analyses of the friction mechanism. A modified classical friction model is proposed, which describes the friction behavior including Stribeck (*i.e.,* pre-sliding) effect. It is also performed an in-depth study for the velocity fields generated at the contact regions along with a Hertzian analysis of deflection. Hertzian results were employed to construct the geometric parameters and normal pressure distributions of the contact surface with respect to elastic and plastic deformations. With analytic formulations of the relative velocity field, deflection, and friction mechanism of the S-CVT and SS-CVT, quantitative analyses of spin loss for each case are carried out. As a result, explicit models of spin loss were developed.

KEY WORDS : Spin loss, Continuously variable transmission, S-CVT, SS-CVT, Friction

1. INTRODUCTION

1.1. Spin Loss of Friction Drive CVT

Slippage takes place whenever the transmitted force (or torque) exceeds the limiting value at the contact points of friction drive CVT. Slippage causes wear, heat, power loss, and even failure of the power transmission; therefore it is a critical problem in the design and control of CVT. Although many efforts have been dedicated to compensate for slip in a variety of mechanical systems or ages, an accurate analysis of the mechanism of slippage is still an open topic of research.

There are two main sources of power loss in friction/traction drive CVT, excluding the losses due to its mechanical structure, bearings and shifting actuator. One is "slip loss" on the contact points between the two rotating bodies resulting from slippage in the rolling directions. Once the rolling directional slippage occurs at these contact points, the transmitted power becomes different from the desired value; the power transmission can even fail. The other one is called "spin loss," which is also one of the main design issues in traction drives also (see Figure 1). Spin loss results from the elastic contact deformation of rotating bodies that have different rotational
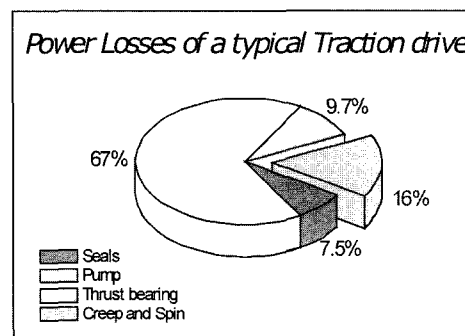

Figure 1. Spin loss in traction drives.

velocities. To reduce the spin loss in traction and friction drives, many designers have investigated different approaches to optimal contact geometry design, normal load application, and controller design (Loewenthal, 1981; Wang, 1989; Tanaka, 1987; Tanaka, 1989; Tanaka, 1991).

1.2. Spherical and Semi-Spherical CVT

In previous studies (Kim, 2002; Cho, 2000), we reported newly developed friction drives: Spherical CVT(S-CVT) and Semi-Spherical CVT(SS-CVT). The S-CVT and SS-CVT both have simple kinematic structures and transmit power via dry rolling friction on the contact points between a sphere and discs. Their compact and simple

*Corresponding author. e-mail: kjungyun@robotics.snu.ac.kr

(a) Standard structure of S-CVT
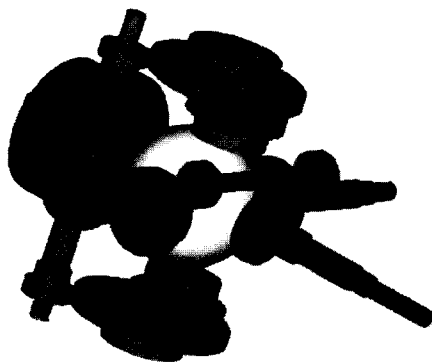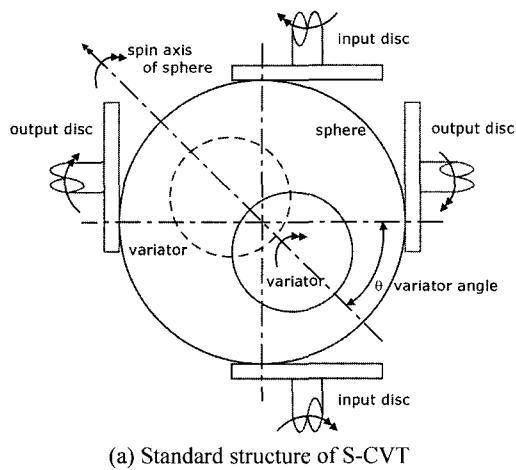

(b) 3-dimensional view

Figure 2. Spherical CVT.

design and relatively simple control make them particularly effective for mechanical systems in which excessively large torques are not required. Moreover, the S-CVT and SS-CVT can realize IVT characteristics, *i.e.*, the ability to transit smoothly between the forward, neutral, and reverse states without the need for any brakes or clutches.

1.2.1. Spherical CVT

The S-CVT is composed of three pairs of input and output discs, variators, and a sphere (see Figure 2).

The input discs are connected to the power source, *e.g.*, an engine or an electric motor, while the output discs are connected to the output shafts. The sphere transmits power from the input discs to the output discs *via* rolling resistance between the discs and the sphere. The variators, which are connected to the shifting controller, are in contact with the sphere like the discs, and constrain the direction of rotation of the sphere to be tangent to the rotational axis of the variator. To transmit power from the discs to the sphere or from the sphere to the discs, a device that supplies a normal force to the sphere, such as a spring or hydraulic actuator, must be installed on each

shaft. In the S-CVT and SS-CVT cases, the normal load is simply supplied by the pre-load of springs.

By varying the axis of rotation of the sphere, it is in turn possible to vary the radius of rotation of the contact point between the input disc and the sphere, as well as the radius of rotation of the contact point between the output disc and the sphere (see more details in Kim, 2002). Assuming roll contact without slip, the speed and torque ratio between the input and output discs is related to the variator angle by the following relations:

$$\frac{\omega_{out}}{\omega_{in}} = \frac{r_i}{r_o}\tan\theta \tag{1}$$

where θ is the angular displacement of the variator, ω_{in} and ω_{out} are the respective angular velocities of the input and output shafts, and r_i and r_o are the respective radii of the contact points of the input and output discs.

1.2.2. Semi-spherical CVT

The SS-CVT is composed of two pairs of output discs and semi-spherical variators. The variators, which are in contact with the output discs, are connected to the power source through an input device, which is a set of bevel gear in this study (see Figure 3).

The variators are also connected to the shifting controller, and constrain the contact point with the output discs to be tangent to the rotational axis of the variator.

By varying the axis of rotation of the variator, it is possible to vary the radius of rotation of the contact point between the output disc and the variator (see more details in Cho, 2000). Assuming roll contact without slip, the speed and torque ratio between the variators and output discs is related to the variator angle by the following relations:

$$\frac{\omega_{out}}{\omega_{in}} = \frac{R}{r_o}\frac{1}{\alpha}\sin\theta \tag{2}$$

where θ is the angular displacement of the variator, ω_{in} and ω_{out} are the respective angular velocities of the input and output shafts, α is the gear ratio of input bevel gear
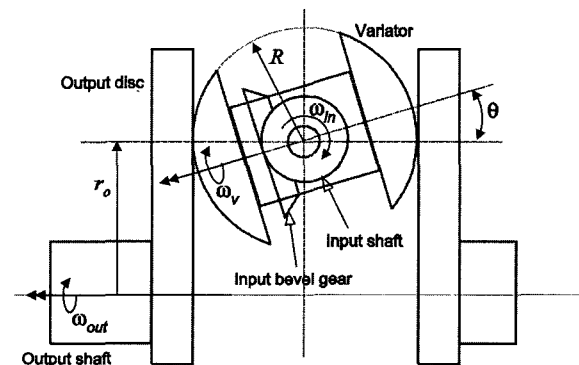

Figure 3. Standard structure of SS-CVT.

set, and R and r_o are the respective radii of the variator and output discs.

2. MODIFIED FRICTION MODEL

Pure rolling friction conditions occur when the contact between two surfaces is a point. However, according to Rabinowicz (1965), the contact region between two surfaces is typically of larger area than a point due to an elastic (and possibly plastic) deformation. Classical friction, also referred to as the stick-slip model, is the earliest and most widely used model of friction. Static friction is the force required to initiate motion from rest. Typically, the magnitude of static friction is greater than that of kinetic friction, which can lead to intermittent motion known as "stick-slip".

Contrary to the predictions derived from the classical friction model, researchers including Courtney-Pratt and Eisner (1957) and others have found experimentally that small relative displacements between two bodies in contact occur when the applied tangential force is less than the static friction. Dahl (1977) provided a model of this pre-sliding displacement phenomenon, known as the "Dahl model," that assumes friction force is a function of displacement x and time t such that

$$\frac{dF_f(x, t)}{dt} = \frac{\partial F_f(x, t)}{\partial x}\dot{x} + \frac{\partial F_f(x, t)}{\partial t} \tag{3}$$

While the simple static plus kinetic friction model offers an intuitive explanation for the possibility of stick-slip oscillations, it does not offer adequate justification for the existence of these limit cycles in the wide range of conditions under which they have been observed. However, several researchers have found a source for this discrepancy in the Stribeck effect, and experimentally derived a model of friction variation with velocity as depicted in Figure 4. The implication of the Stribeck
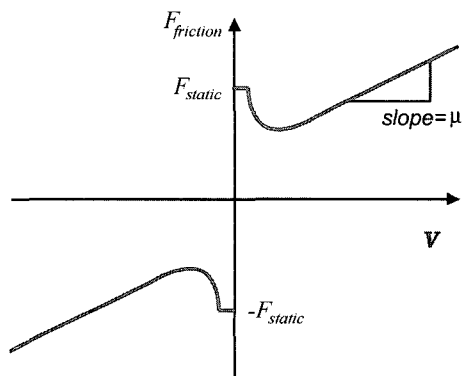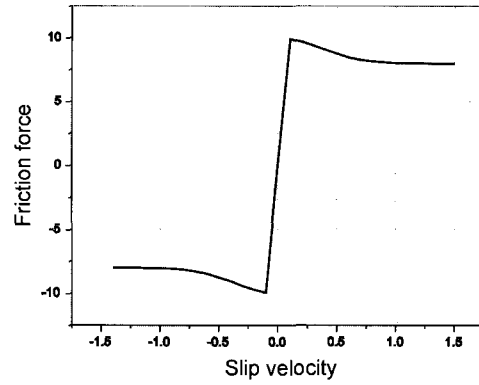

Figure 4. Stribeck effect.

Figure 5. Proposed friction model.

effect for servomechanism dynamics includes an increased likelihood of stick-slip limit cycling at low velocities. Among many empirical models derived for the friction incorporating the Stribeck effect, the following is the most popular:

$$F_f(V) = F_k \cdot \text{sgn}(V) + \mu V + (F_s - F_k)e^{-(V/V_{str})^2} \cdot \text{sgn}(V) \tag{4}$$

where V_{str} is the critical Stribeck velocity.

Friction models based on Dahl's show difficulties in numerical integration due to the high stiffness and damping coefficients; moreover they must be obtained through a careful experimental analysis (Lee, 1999). Thus, the classical stick-slip friction model is adopted in this paper, because velocity reversal seldom occurs in friction drive CVTs. We propose a modified classical friction model including Stribeck effect like

$$F_f = \left[(\mu_s - \mu_k)\exp\left\{-\left(\frac{\Delta V}{V_{str}}\right)^2\right\} + \mu_k\right]P \cdot \text{sgn}(\Delta V) \tag{5}$$

where μ_s, μ_k are static and kinetic coefficients of friction, respectively. Here we neglect viscous friction, as there is no lubricant layer in friction drive CVTs. For typical values of friction model parameters, the friction force versus slip velocity of the proposed model is depicted in Figure 5.

3. VELOCITY FIELDS ON THE CONTACT SURFACE

The friction force on the contact surface is determined by the normal force and friction coefficients. Considering that the kinetic coefficient of friction is related to the relative velocity ΔV between two rotating bodies, we first investigate the relative velocity field on the contact surface. In this section, Hertzian results for elastic deflection are employed to construct the geometric parameters of
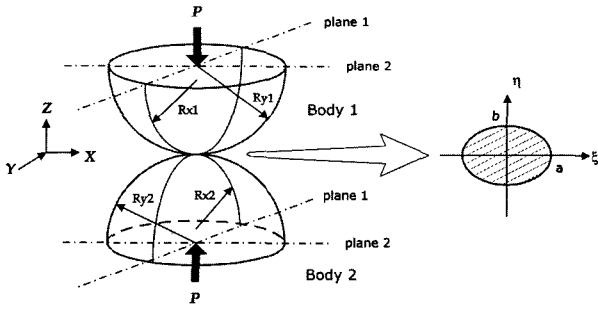
Figure 6. Contact of two bodies with different curvature.

the contact surface. Hertzian theory deals with the general solution of the elastic contact problem of rigid bodies (Timoshenko, 1951; Chung, 1996).

3.1. Contact of Rotating Bodies with Different Radii of Curvature

Consider two solid bodies in contact under a normal force P (Figure 6). In this figure, R_{x1}, R_{y1} and R_{x2}, R_{y2} denote their radii of curvature respectively. The material properties (e.g., Young's modulus and Poisson's ratio) of each body are E_1, n_1 and E_2, n_2 respectively. We set the reference frame **XYZ** to be on the contact point, and the local coordinate frame $\{\xi\eta z\}$ on the deformed contact surface such that its origin coincides with the contact center. According to Hertzian analysis (Chung, 1996), the contact surface in this case produces an elliptic shape with principal axes a, b and corresponding normal deflections δ_x, δ_y; these can be approximated as

$$a = 1.109 \times \sqrt{\frac{P}{E} \cdot \frac{R_{y1}R_{y2}}{R_{y1} + R_{y2}}},$$
(6)

$$b = 1.109 \times \sqrt{\frac{P}{E} \cdot \frac{R_{x1}R_{x2}}{R_{x1} + R_{x2}}},$$

$$\delta_x = 2.64 \times \sqrt{\frac{P^2}{E^2} \cdot \frac{R_{x1} + R_{x2}}{R_{x1}R_{x2}}},$$
(7)

$$\delta_y = 2.64 \times \sqrt{\frac{P^2}{E^2} \cdot \frac{R_{y1} + R_{y2}}{R_{y1}R_{y2}}},$$

$$\frac{2}{E} = \frac{(1 - v_1^2)}{E_1} + \frac{(1 - v_2^2)}{E_2}$$
(8)

where E is the equivalent Young's modulus.

Suppose that body 1 and body 2 have angular velocities ω_1 and ω_2, respectively. Here we assume that the contact center does not dislocate from the original contact center (i.e., roll without slip in the rolling direction). Then we can derive the relative velocity field $\Delta V(x, h) = V_1(\xi, \eta) - V_2(\xi, \eta)$ in the contact surface with pure rotational motion in $\mathbf{R}^3$, using the relevant curvature radii as follows:
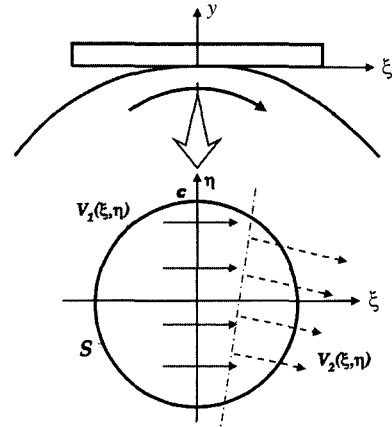

Figure 7. Velocity vector field on contact point.

$$\Delta V(\xi, \eta) = \begin{bmatrix} \left(R_{y1} - \frac{\delta_y}{2}\right)\omega_{1Y} - \left(R_{y2} - \frac{\delta_y}{2}\right)\omega_{2Y} \\ + \eta(\omega_{1Z} - \omega_{2Z}) \\ \left(R_{x1} - \frac{\delta_x}{2}\right)\omega_{1X} - \left(R_{x2} - \frac{\delta_x}{2}\right)\omega_{2X} \\ + \xi(\omega_{1Z} - \omega_{2Z}) \end{bmatrix}$$
(9)

where $\omega_{iX, Y, Z}$ is the rotational velocity component in the reference frame of each body.

Taking into account that the two contact bodies in the S-CVT and SS-CVT are disc and sphere, one can let $R_{x1} = R_{y1} = infinity$ and $R_{x2} = R_{y2} = R$ in Equations (6)-(9). Furthermore, supposing there is no bending deformation of the variator along the x, z axes, the normal deflection δ and contact surface radius c can be calculated as

$$c = 1.109 \times \sqrt[3]{\frac{P}{E} \cdot R}, \qquad \delta = 2.64 \times \sqrt[3]{\frac{P^2}{E^2} \cdot \frac{1}{R}}$$
(10)

3.2. Spherical CVT

Figure 7 shows the contact surface between the sphere and upper variator. In this figure, we set a local coordinate frame $\{\xi y \eta\}$, at the center of the contact surface S; the rolling direction is in the x direction.

To obtain each velocity field, we first recall that the sphere has a pure rotational speed of ω in the η direction and the variator a rotational speed of ω_v in the y direction. The velocity field of the sphere $V_1(\xi, \eta)$ and that of variator $V_2(\xi, \eta)$ on the contact surface can be obtained as follows:

$$V_1(\xi, \eta) = [(R - \delta)\omega, 0],$$

$$V_2(\xi, \eta) = [(\varepsilon + \eta)\omega_v, -\xi\omega_v]$$

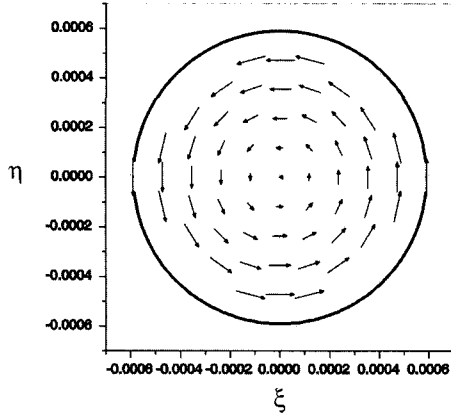where ε is the distance between the contact surface center

Figure 8. Typical relative velocity vector diagram.

and variator center. Consequently, the relative velocity field $\Delta V_\nu(\xi, \eta)$ can be derived as

$$\Delta V_\nu(\xi, \eta) = [(R - \delta)\omega - (\varepsilon + \eta)\omega_\nu, -\xi\omega_\nu] \qquad (11)$$

Similarly, the relative velocity fields at the other contact points (input and output discs) can be obtained.

As shown in Equation (11), there is a relative velocity component of ΔV_ν in the η direction, ΔV_η, on the contact surface. However $\Delta V_\eta(\xi, \eta)$ does not accumulate total relative velocity in the η direction, because it is symmetric along the η axis. Therefore, $\Delta V_\eta(\xi, \eta)$ contributes to spin along the direction normal to the $\xi\eta$ plane. In the case of $\Delta V_\xi(\xi, \eta)$, the relative speed of $(\delta\omega + \eta\omega)$ occurs in the rolling direction (recall the rotational speed relation of $R\omega = \varepsilon\omega_\nu$). Note that δ becomes small enough to be neglected compared R (for example, $\delta = 2.4\times10^{-3}$ mm, $c = 0.59$ mm, and $R = 30$ mm for the case of the S-CVT prototype); therefore $\Delta V_\xi(\xi, \eta)$ can be approximated to be $-\varepsilon\omega_\nu$. The contribution of $\Delta V_\xi(\xi, \eta)$ is also a spin, similar to $\Delta V_\eta(\xi, \eta)$.

The vector diagram of relative velocity is obtained using typical values of ω_j, ω_ν, ε, R, P, and E that
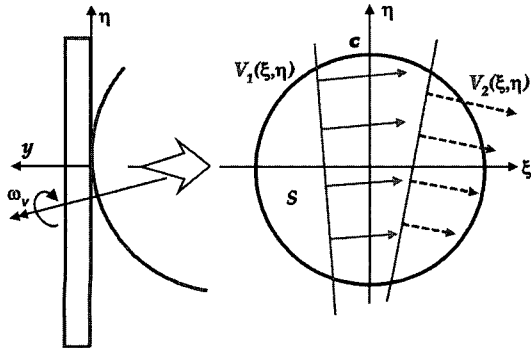

Figure 9. Velocity vector field on contact point.

correspond to the S-CVT prototype specification (see Figure 8).

3.3. Semi-spherical CVT

Figure 9 shows the contact surface between the output disc and variator. Like the S-CVT case, we set a local coordinate frame $\{\xi y\eta\}$ at the center of the contact surface S, in this figure.

Unlike the S-CVT case, the variator has an angular velocity ω_ν not only in the y direction; ω_ν lies in the ηy plane with the angular offset of θ (see Figure 3). Therefore, the velocity field of the variator $V_1(\xi, \eta)$ and that of output disc $V_2(\xi, \eta)$ on the contact surface can be obtained as follows:

$$V_1(\xi, \eta) = [(R\sin\theta + \eta\cos\theta)\omega_\nu, -\xi\omega_\nu],$$
$$V_2(\xi, \eta) = [(r_o + \eta)\omega_{out}, -\xi\omega_{out}]$$

where R is the radius of variator, and r_o is the distance between the contact surface center and the output disc center. And here we neglect again δ for it is small compared to R. Consequently, the relative velocity field $\Delta V_\nu(\xi, \eta)$ can be derived.

There could be existed torque losses on the contact point in the SS-CVT, because the rotational axis of variator has an angular offset of θ to the normal contact surface. This torque loss also occurs in toroidal type traction drives, which is called as "spin torque loss," for their contact geometries and shifting mechanisms. In many CVT designs having the similar shifting mechanisms with SS-CVT, the "spin loss" includes these torque losses. However, this kind of torque loss does not occur in the S-CVT case, considering the sphere has a pure rotational speed of ω in the η direction. Therefore we will not consider these torque losses in this study for the comparison with the S-CVT case.

From the fact that $R\omega_\nu \sin\theta = r_o\omega_{out}$, which is resulted from the rolling condition in contact points, the relative velocity $\Delta V_\xi(\xi, \eta)$ can be reduced as
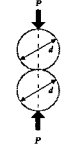
$$\Delta V_\nu(\xi, \eta) = [\eta(\omega_\nu\cos\theta - \omega_{out}), \xi(\omega_{out} - \omega_\nu)] \qquad (12)$$

Similar to the S-CVT case, the spin velocity field can be found straightforwardly, although there are no excessive forces that cause slippage. From these results, we can be assured that there must be spin in the contact surface around the origin of the local coordinate frame of the contact point in the S-CVT and SS-CVT, regardless of the existence of shear force resulting slippage.

4. NORMAL PRESSURE DISTRIBUTION

Now we consider the normal pressure distribution on the contact patch to obtain the friction force as well as to analyze the strength of the S-CVT and SS-CVT. The normal pressures on S-CVT and SS-CVT are applied by

Table 1. Maximal normal pressure comparison.

$$\alpha = 1.109\sqrt[3]{\frac{P}{E} \cdot \frac{r_1 r_2}{r_1 + r_2}} \qquad \delta = 2.46\sqrt[3]{\frac{P^2}{E^2} \cdot \frac{r_1 + r_2}{r_1 r_2}}$$

$$p_{mean} = \frac{P}{\pi\alpha^2} = \frac{1}{1.109^2 \pi}\sqrt[3]{PE^2 \cdot \left(\frac{r_1 + r_2}{r_1 r_2}\right)^2}$$

$$p_{max} = 1.5 p_{mean} = 0.388\sqrt[3]{PE^2 \cdot \left(\frac{r_1 + r_2}{r_1 r_2}\right)^2}$$

$$p_{max} = 0.388\sqrt[3]{\frac{16 P E^2}{d^2}}$$

$$p_{max} = 0.388\sqrt[3]{\frac{PE^2}{d^2}}$$

$$p_{max} = 0.388\sqrt[3]{\frac{4 P E^2}{d^2}}$$

the pre-set of load spring, and they are not varied with the input torque. A Hertzian pressure distribution develops in the circular shaped contact patch (with radius c) between the sphere and disc. The pressure at each point in the contact surface is known to be

$$p(\xi, \eta) = \frac{3}{2}\frac{P}{\pi c^3}\sqrt{c^2 - \xi^2 - \eta^2} \qquad (13)$$

The maximal normal pressure p_{max} is located at the center of the contact surface; at the boundaries, the normal pressure p becomes zero. The mean value of normal pressure, p_{mean}, equals the normal contact force P divided by the area of the contact surface:

$$p_{mean} = \frac{P}{\pi c^2} = \frac{1}{1.109^2 \pi}\sqrt[3]{\frac{PE^2}{R^2}}$$

Using the relation $p_{max} = 1.5 p_{mean}$, the maximal normal pressure can be calculated as

$$p_{max} = 0.388\sqrt[3]{\frac{PE^2}{R^2}}$$

The maximal pressure p_{max} should not exceed the yield strength of the sphere and disc. For design purposes, the maximal normal pressure values for several combinations of contact bodies are illustrated in Table 1.

On the same load condition, the maximal pressure values for the S-CVT and SS-CVT (i.e., sphere and disc contact) reaches almost 1.588 times that of the case that is

inscribed in a circular body more than twice the radius.

5. NUMERICAL RESULTS

Relative velocities resulting from the elastic contact of rotating bodies usually give rise to friction mechanisms; in which case friction moments (spin loss) occur in the contact region. Consider the infinitesimal area at the contact surface S, with the friction force of the i th area in the rolling direction (ξ direction) denoted $F_{\xi i}$, and $F_{\eta i}$ the force in the η direction. Recall that the normal pressure distribution has symmetries along the ξ and η axes, and that ΔV_ξ varies along the η direction, and ΔV_η along the x direction; there are no total relative velocities in the ξ and η directions. Therefore one can conclude that the total friction force F_ξ and F_η become zero in both S-CVT and SS-CVT.

Using the proposed friction model in Equation (5), the spin moment T_{spin} can be calculated as

$$T_{spin} = \int_{-c}^{c}\int_{-c}^{c}(\eta F_{\xi i} + \xi F_{\eta i})d\xi d\eta \qquad (14)$$

5.1. Spherical CVT
Recall that the relative velocity ΔV in S-CVT: $\Delta V_\xi = -\eta\omega_v$, $\Delta V_\eta = \xi\omega_v$. Rearranging and integrating by parts, Equation (14) becomes

$$T_{spin} = \frac{3Pc}{4\pi}\left[\mu_k + (\mu_s - \mu_k)\frac{2}{c^4}\frac{V_{str}^2}{\omega_v^2}\right.$$
$$\left.\left[c^2 - \frac{V_{str}^2}{\omega_v^2}\left(1 - \exp\left\{-\left(\frac{c\omega_v}{V_{str}}\right)^2\right\}\right)\right]\right] \qquad (15)$$

To investigate the amount of spin loss at the contact points of the S-CVT, we calculate the respective spin losses using Equation (15) for the input and output discs and variators with typical values of μ_k, μ_s, V_{str}, P.
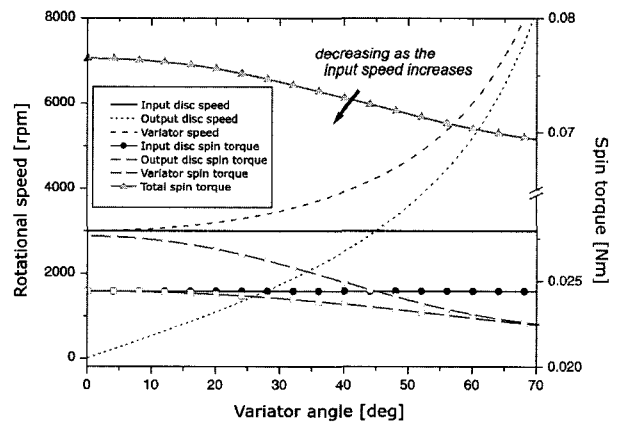

Figure 10. Spin losses on S-CVT at input speed of 3000 rpm.

Figure 10 shows the numerical results for spin loss at an input speed of 3000 rpm along the variator angle change, and the speed changes in the discs and variator. Spin moments occur at six contact regions in the S-CVT, and the total amount of spin loss reaches almost 0.076 *Nm*. Spin moments decrease as the variator angle increases, except for the input discs whose spin moments remain constant (because there are no speed changes in the input discs). The gross spin loss decreases as the input speed rises, that is due to the characteristics of our friction model: the friction force at zero relative speed has the maximal value.

5.2. Semi-spherical CVT

Rearranging and integrating by parts, Equation (14) becomes in the SS-CVT case

$$T_{spin} = \frac{3Pc}{8\pi}\left[\mu_k + (\mu_s - \mu_k)\frac{2}{c^4}\frac{V_{str}^2}{\omega_\xi^2}\right.$$

$$\left[c^2 - \frac{V_{str}^2}{\omega_\xi^2}\left(1 - \exp\left\{-\left(\frac{c\omega_\xi}{V_{str}}\right)^2\right\}\right)\right]\right]$$

$$+ \frac{3Pc}{8\pi}\left[\mu_k + (\mu_s - \mu_k)\frac{2}{c^4}\frac{V_{str}^2}{\omega_\eta^2}\right.$$

$$\left[c^2 - \frac{V_{str}^2}{\omega_\eta^2}\left(1 - \exp\left\{-\left(\frac{c\omega_\eta}{V_{str}}\right)^2\right\}\right)\right]\right] \qquad (16)$$

where, $\omega_\xi = \omega_v\cos\theta - \omega_{out}$ and $\omega_\eta = \omega_{out} - \omega_v$. We calculate the respective spin losses for the output discs and variators with the same values of μ_k, μ_s, V_{str}, P in the S-CVT case. Here we set the gear ratio α to one: $\omega_v = \omega_{in}$.

Figure 11 shows the numerical results for spin loss at an input speed of 3000 rpm along the variator angle change, and the speed change in the output disc. Spin moments occur at four contact regions in the SS-CVT, and the total amount of spin loss reaches almost 0.1 *Nm*.
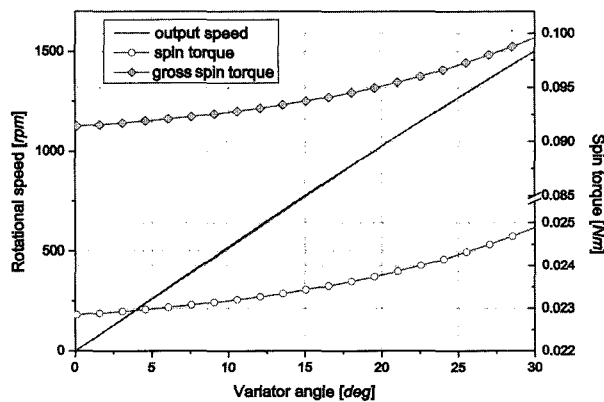

Figure 11. Spin losses on SS-CVT at input speed of 3000 rpm.

Contrary to the S-CVT case, spin moments increase as the variator angle increases.

The average values of spin loss of our numerical results are 0.072 *Nm* in the S-CVT case and 0.093 *Nm* in the SS-CVT. Considering the input torque is limited under the static friction torque of 1.962 *Nm*, the ratios of spin loss to static friction torque are almost 3.67% in the S-CVT case and 4.6% in the SS-CVT. Considering normal operating conditions, at which the input torque is smaller than the limiting torque, one can note that the ratios of spin loss become much greater. Furthermore, the S-CVT is advantageous to reduce the spin loss and obtain a wide range of shifting ratio, *i.e.*, variator angle. To reduce this loss by operating conditions, it is helpful to operate the S-CVT and SS-CVT with high input speeds; the increased relative velocity reduces the relevant friction force.

6. CONCLUSIONS

This paper has presented the spin loss analysis of friction drive CVTs, especially for the cases of S-CVT and SS-CVT. The S-CVT and SS-CVT can realize the infinitely variable transmission characteristics. And their compact and simple designs and relatively simple control make them particularly effective for mechanical systems in which excessively large torques are not required. There are two main sources of power loss resulting from slippage in the friction drive CVTs, spin and slip loss. Spin loss, which is also a main design issues in traction drives, results from the elastic contact deformation of rotating bodies having different rotational velocities.

We first review briefly the structure and operating principles of the S-CVT and SS-CVT. And to analyze the losses resulting from slippage, we reviewed previous analyses of the friction mechanism. A modified classical friction model is proposed, that describes the friction behavior including Stribeck (*i.e.*, pre-sliding) effect. We also performed an in-depth study for the velocity fields generated at the contact regions along with a Hertzian analysis of deflection. Hertzian results were employed to construct the geometric parameters and normal pressure distributions of the contact surface with respect to elastic and plastic deformations.

With analytic formulations of the relative velocity field, deflection, and friction mechanism of the S-CVT and SS-CVT, we carried out quantitative analyses of spin loss for each case. As a result, explicit models of spin loss were developed. From the numerical results with typical values of material properties and load conditions, we can conclude the spin loss of S-CVT case is smaller than that of SS-CVT. Furthermore, the spin loss of SS-CVT increases contrary to the fact that that of S-CVT decreases as the variator angle change increases.

REFERENCES

Cho, H., Kim, J., Jeon, S., Lee, J., Kim, J. and Park, Y. (2000). Development of a hybrid electric vehicle equipped with semi-spherical CVT. *Proc. 2000 KSAE Spring Conference* **I**, 349-354, April 28-29, Seoul, Korea.

Chung, S. and Han, D. C. (1996). *Standards of Mechanical Design*, Dongmyung-Sa, Korea.

Courtney, J. and Eisner, E. (1957). The effect of a tangential force on the contact of metallic bodies. *Proc. the Royal Society* **A238**, 529-550.

Dahl, P. R. (1977). Measurement of solid friction parameters of ball bearing. *Proc. the 6th Annual Sym- posium on Incremental Motion, Control Systems and Devices*, 49-60, University of Illinois.

Druten, V. R. M., Tilborg, P. G.·V., Rosielle, P. C. J. N. and Schouten, M. J. W. (2000). Design and construction aspects of a zero inertia CVT for passenger cars. *International Journal of Automotive Technology* **1**, **1**, 42-47.

Kim, J., Park, F. C., Park, Y. and Shizou, M. (2002). Analysis and control of a spherical continuously variable transmission. *Journal of Mechanical Design* **124**, **1**, 21-29.

Lee, C. (1999). Comparison of friction model on the variable DOF system. *Proc. 1999 KSME Spring Conference* **3**, 134-140, Taegu, Korea.

Loewenthal, S. H. (1981). Evaluation of a high performance fixed-ratio traction drive. *Trans. ASME* **103**.

Rabinowicz, E. (1965). *Friction and Wear of Materials*, John Wiley and Sons. New York.

Tanaka, H. (1987). Power transmission of a cone rollertoroidal traction drive (2nd report, side slip and speed ratio change). *Journal of JSME* **87–1138** A.

Tanaka, H. (1989). Spin moment of a thrust ball bearing in traction fluid. *Journal of JSME* **89–0148 B**.

Tanaka, H., Eguchi, M. (1991). Speed ratio control of a half-toroidal traction drive CVT. *Journal of JSME* **91–0375 B**.

Timoshenko, S. and Goodier, J. N. (1951). *Theory of Elasticity*, 2nd Ed., McGraw-Hill Book Co., New York.

Wang, B. T. and Fries, R. H. (1989). Determination of creep force, moment, and work distribution in rolling contact with slip. *Trans. ASME* **111**, Oct.